Available online at www.sciencedirect.com
SCIENCE DIRECT
Intermetallics 14 (2006) 630–638
Intermetallics
www.elsevier.com/locate/intermet

Infrared brazing of $Ti_{50}Ni_{50}$ shape memory alloy using two Ag–Cu–Ti active braze alloys

R.H. Shiue, S.K. Wu *

Department of Materials Science and Engineering, National Taiwan University, Taipei 106, Taiwan, ROC

Received 30 June 2005; accepted 24 October 2005
Available online 4 January 2006

Abstract

Microstructural evolution, shape memory effect and shear strength of infrared brazed $Ti_{50}Ni_{50}$ shape memory alloy using Cusil-ABA® and Ticusil® active braze alloys are investigated. The Ag–Cu eutectic braze alloy can readily wet $Ti_{50}Ni_{50}$ substrate by minor titanium additions. The brazed $Ti_{50}Ni_{50}$/Cusil-ABA®/$Ti_{50}Ni_{50}$ joint is mainly comprised of Cu-rich, Ag-rich and CuNiTi phases. On the other hand, the brazed $Ti_{50}Ni_{50}$/Ticusil®/$Ti_{50}Ni_{50}$ joint consists of Ag-rich, Cu-rich and $TiCu_2$ phases. Because the chemical composition of Ticusil braze alloy is located inside the huge miscibility gap, the molten braze tends to be separated into two liquids during brazing. One is rich in Ag, and the other is rich in both Cu and Ti. The Ag-rich liquid does not react with $Ti_{50}Ni_{50}$ substrate. In contrast, the copper content is depleted from the matrix of brazed joint due to the formation of interfacial $TiCu_2$ phase. The $TiCu_2$ phase is less detrimental to the shape memory effect than CuNiTi phase during the shape recovery bending test. Shear strength of brazed joints exceeds 200 MPa for both braze alloys if the brazing time exceeds 180 s. However, thick interfacial CuNiTi and $TiCu_2$ layers can deteriorate the shear strength.

Keywords: A. Intermetallics, miscellaneous; B. Bonding; C. Joining; D. Microstructure; B. Phase diagrams

1. Introduction

Equiatomic $Ti_{50}Ni_{50}$ shape memory alloy (SMA) is well known for its superior shape memory effect and pseudo-elasticity [1,2]. In addition, its high corrosion resistance and biocompatibility make $Ti_{50}Ni_{50}$ SMA an excellent candidate for medical safety and robotics applications [3–5].

To join $Ti_{50}Ni_{50}$ SMA successfully without detrimental to the characteristic of shape memory effect can extend its application. Different from the welding process, the base metal is essentially not melted during the brazing process. It is possible to braze $Ti_{50}Ni_{50}$ SMA without melting the base metal in order to keep its shape memory effect. Compared with the traditional furnace brazing, infrared brazing is suitable in studying the mechanism and microstructural evolution of the joint with the advantage of its rapid heating rate as high as 3000 °C/min. Thus, infrared brazing has been applied to investigate the kinetics of brazing process in recent years [6,7].

The selection of filler metal plays a crucial role in brazing $Ti_{50}Ni_{50}$ SMA. The wettability of the braze alloy, the mechanical properties of the brazed joint and the formation of intermetallic phases at the joint must all be considered in the selection of the filler metal. It is reported that the existence of Ti(Cu,Ni) phase, instead of CuNiTi phase, in the brazed joint is beneficial to preserve the shape memory effect of the infrared brazed $Ti_{50}Ni_{50}$ SMA with copper thin foil [8]. The commercial Ag–Cu eutectic braze alloy (BAg-8) is well known for its use in joining copper alloys, stainless steels and nickel-base alloys. Although the solubility of silver is almost zero in $Ti_{50}Ni_{50}$ alloy [9], the solubility of copper in $Ti_{50}Ni_{50}$ alloy is rather higher [10]. It is also reported that the wettability of Ag–Cu eutectic braze can be significantly improved with the addition of 1–5 wt% titanium [11,12]. Accordingly, it is possible to infrared brazing $Ti_{50}Ni_{50}$ alloy using the silver-based braze alloy with the addition of minor amount of titanium.

In this study, infrared joining of $Ti_{50}Ni_{50}$ SMA using two silver-based braze alloys by adding different amount of titanium is studied. The wettability, microstructural evolution, shear strength and shape memory effect of infrared brazed joints are comprehensively evaluated in order to unveil the relationship between the microstructure and the performance of the brazed joints.

* Corresponding author. Tel.: +886 2 2363 7846; fax: +886 2 2363 4562.
E-mail address: skw@ntu.edu.tw (S.K. Wu).

0966-9795/$ - see front matter © 2005 Elsevier Ltd. All rights reserved.
doi:10.1016/j.intermet.2005.10.012

2. Experimental procedure

$Ti_{50}Ni_{50}$ SMA was prepared by vacuum arc remelting (VAR) of titanium rods (purity: 99.7 wt%) and nickel pellets (purity: 99.9 wt%). Both titanium rods and nickel pellets were cleaned by $1HF–15HNO_3-64H_2O$ (in ml) and saturated NaOH solution prior to performing VAR. Both Cusil-ABA® and Ticusil® foils purchased from Wesgo® Metals were used in brazing. The thickness of braze alloys was 50 μm throughout the experiment. Chemical compositions, and solidus and liquidus temperatures of braze alloys are listed in Table 1.

The infrared furnace used in this study was ULVAC SINKO-RIKO RHL-P610C with the maximum heating rate of about 3000 °C/min. Infrared brazing was performed under 5×10^{-5} mbar vacuum, and the heating rate was set at 900 °C/min throughout the experiment. All specimens were preheated at 600 °C for 60 s to equilibrate the actual temperature in the specimen. The process variables used in this study are listed in Table 2.

The size of brazed specimens was $10.0\times10.0\times2.5$ mm^3. All joined surfaces were polished by SiC papers to grit 600 and ultrasonic cleaned by acetone before infrared brazing. The area of the filler metal foil was approximately the same as that of the base metal. The graphite fixture was used in this study to enhance the absorption of infrared rays during infrared brazing.

Table 1
Solidus and liquidus temperatures of braze alloys

Braze alloy	Cusil-ABA®	Ticusil®
Solidus (°C)	780	830
Liquidus (°C)	815	850
Composition (wt%)	63Ag–35.25Cu–1.75Ti	68.8Ag–26.7Cu–4.5Ti

Table 2
Summary of process variables used in the experiment

Temperature (°C)	Brazing time (s)	Cusil-ABA® braze alloy	Ticusil® braze alloy
840	15	M	–
840	60	M/S	–
840	90	M	–
840	180	M/S	–
840	300	M/B/S	–
870	15	M	M
870	60	M/S	M/S
870	90	M	M
870	180	M/S	M/S
870	300	M/S/W	M/S/B/W
900	15	M	M
900	60	M/S	M/S
900	90	M	M
900	180	M/S	M/S
900	300	M/S/W	M/S/W
930	15	–	M
930	60	–	M/S
930	90	–	M
930	180	–	M/S
930	300	–	M/S/W

M, metallurgical observation specimen; S, shear test specimen; B, bending test specimen; W, wetting angle test specimen.

Specimens were sandwiched between two graphite plates, and an R-type thermocouple in the upper graphite plate was contacted with the brazed specimen [8].

The schematic diagram of graphite fixture used for the shear test is shown in Fig. 1, in which two black bold lines between $Ti_{50}Ni_{50}$ base metals are the braze alloys with the width of approximately 1.5 mm. Shear tests of infrared brazed joints were performed using a Shimadzu AG-10 universal testing machine. The infrared brazed specimen was compressed with a constant speed of 1 mm/min. The Philips PW1710 X-ray diffractometer (XRD) with Cu K_α X-ray source was used to analyze the structure of fracture surface after the shear test. The cross-section of the brazed joint was examined using a Philips XL-30 scanning electron microscope (SEM) equipped with an energy dispersive spectrometer (EDS). Quantitative chemical analyses were performed using a JEOL JXA 8600SX electron probe microanalyzer (EPMA) equipped with a wavelength dispersive spectrometer (WDS) with a spot size of 1 μm and an operational voltage of 20 kV.

The shape memory effect was evaluated by bending test as shown in Fig. 2. The shape recovery ratio of the infrared brazed joint was obtained in the bending test [13]. The dimensions of the samples used for bending test was machined into 60.0×5.0 mm^2 and 0.5 mm in thickness. The specimen was initially bent to θ_i in liquid nitrogen (77 K). Next, the specimen's temperature was increased to 130 °C in order to measure the shape recovery angle (θ_f). The shape recovery ratio of the joint was defined by $(\theta_i-\theta_f)/\theta_i$ to evaluate its shape memory effect. Additionally, the shape recovery ratio of $Ti_{50}Ni_{50}$ base metal with the same specimen size was also tested for the purpose of comparison.

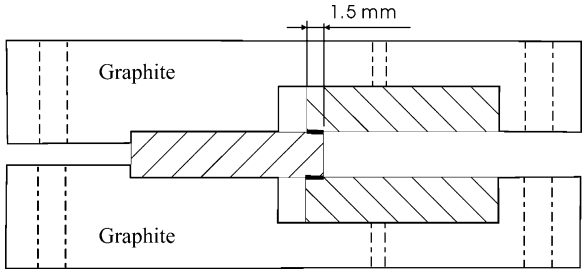

Fig. 1. The schematic diagram of shear test specimen with graphite fixture.

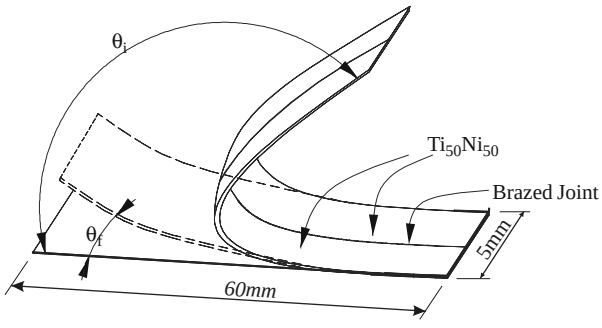

Fig. 2. The schematic diagram of bending test specimen to measure the shape recovery ratio [8].

3. Results and discussion

3.1. Wetting angle of filler alloys with $Ti_{50}Ni_{50}$ substrate

Dynamic wetting angles were measured in the sessile drop test using approximately 0.12 g BAg-8, Ticusil® and Cusil-ABA® filler alloys with near spherical shape on the $Ti_{50}Ni_{50}$ substrate. They were heated up to a specified temperature and held for 0–300 s. Fig. 3 shows the dynamic wetting angle measurements of Ag–Cu eutectic (BAg-8), Cusil-ABA® and Ticusil® braze alloys on $Ti_{50}Ni_{50}$ substrate at various temperatures for 0–300 s. As depicted in Fig. 3, the Ag–Cu eutectic braze alloy is completely dewetted from the TiNi substrate, however, both Ticusil® and Cusil-ABA® alloys demonstrate great improvement in wetting the TiNi substrate. Thus, $Ti_{50}Ni_{50}$ can be effectively wetted by Ag–Cu braze alloy with minor titanium addition. Upon increasing the test temperature from 870 to 900 °C, the wetting angles of both Ticusil® and Cusil-ABA® braze alloys decrease. This characteristic will be further discussed in the following microstructural observation of the brazed joints.

3.2. Microstructural evolution of $Ti_{50}Ni_{50}$/Cusil-ABA®/$Ti_{50}Ni_{50}$ infrared brazed joint

Fig. 4(a)–(e) shows the SEM backscattered electron images (BEIs) of $Ti_{50}Ni_{50}$/Cusil-ABA®/$Ti_{50}Ni_{50}$ specimen infrared brazed at 870 °C for 15, 60, 90, 180 and 300 s, respectively. Most of the brazed region is with eutectic Ag–Cu which primarily consists of Ag-rich and Cu-rich phases. The SEM observations revealed that silver does not react with the substrate and the white Ag-rich matrix is not in contact with the substrate during infrared brazing. There is an interfacial reaction layer in between braze alloy and substrate. According to Fig. 4, widths of the brazements are less than the original thickness of the Cusil-ABA® foil (50 μm) due to the overflow of the molten braze out of the joint during infrared brazing.

Fig. 4 also shows the EPMA results of Fig. 4(e). In Fig. 4(e), there is one continuous reaction layer formed close to $Ti_{50}Ni_{50}$ substrate, as marked by A. The chemical composition of layer A consists of copper, titanium and nickel. According to the isothermal section of ternary Cu–Ni–Ti phase diagram as illustrated in Fig. 5, the stoichiometry of layer A is close to the CuNiTi phase [14]. The CuNiTi phase can also be expressed as $(Cu_xNi_{1-x})_2Ti$ where x ranges from 0.23 to 0.75 [14]. Areas B and C in Fig. 4(e) are the copper-rich phase and the Ag-rich matrix, respectively. The binary phase diagrams of Ag–Cu and Cu–Ti show the highest solubility of silver and titanium in the copper is 5 and 8 at.%, respectively [15]. It is consistent with the current EPMA result of the copper-rich phase (Area B) alloyed with 4.2 at.% Ag and 6.0 at.% Ti. According to the experimental observation, higher brazing temperature, e.g. 900 °C, can accelerate the formation of a thicker CuNiTi reaction layer.

3.3. Microstructural evolution of $Ti_{50}Ni_{50}$/Ticusil®/$Ti_{50}Ni_{50}$ infrared brazed joint

Both the solidus and liquidus temperatures of Ticusil® alloy are higher than those of Cusil-ABA®. Accordingly, higher brazing temperatures are performed in brazing $Ti_{50}Ni_{50}$ substrate using Ticusil® filler alloy. Fig. 6(a)–(e) shows the SEM BEIs of $Ti_{50}Ni_{50}$/Ticusil®/$Ti_{50}Ni_{50}$ specimen infrared brazed at 900 °C for 15, 60, 90, 180 and 300 s, respectively. The EPMA results for the specimen in Fig. 6(e) are also included in Fig. 6. The braze joint consists of Ag-rich and Cu-rich phases, and the silver does not react with the $Ti_{50}Ni_{50}$ substrate. It is obvious that the distribution of Cu-rich phase using Ticusil® braze alloy is different from that using Cusil-ABA® braze alloy. The Cu-rich phase is consumed rapidly even at the initial stage of brazing. It indicates that more vigorous reaction occurs in the Ticusil® brazed joint than in the Cusil-ABA® one.

There is a continuous interfacial layer close to $Ti_{50}Ni_{50}$ substrate, as marked by A in Fig. 6(e). According to the EPMA results, layer A can be identified as $TiCu_2$. It is reported that the Ni atoms can be replaced by Cu atoms in $Ti_{33}Ni_{67-x}Cu_x$ and its structure can vary from $MoSi_2$ structure of CuNiTi phase to

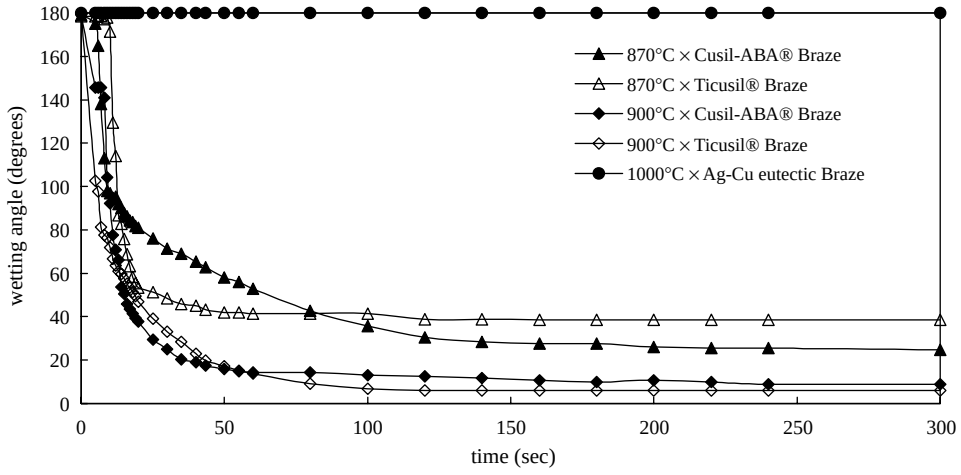

Fig. 3. The dynamic wetting angle measurement of different braze alloys on $Ti_{50}Ni_{50}$ substrate.

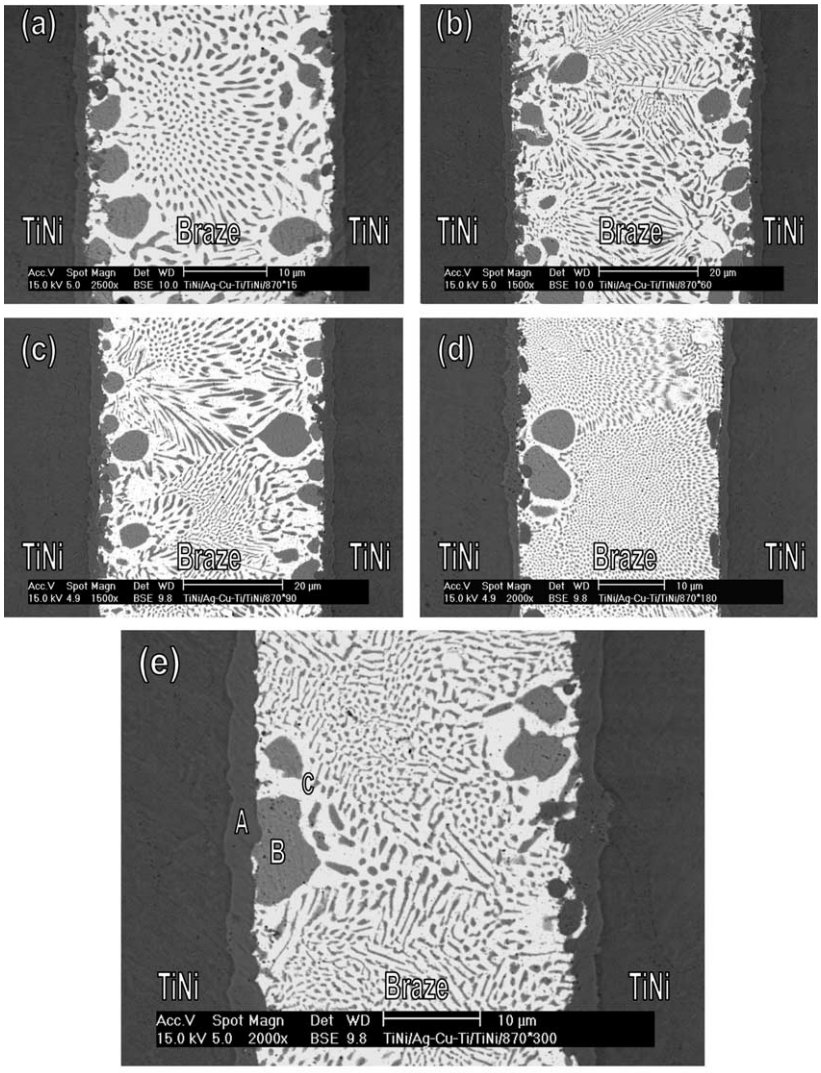

Element (at%)	Cu	Ag	Ti	Ni	Possible phase
A	43.3	--	33.1	23.6	CuNiTi
B	89.8	4.2	6.0	--	Cu-rich
C	12.4	87.6	--	--	Ag-rich

Fig. 4. SEM BEIs and EPMA chemical analysis results of $Ti_{50}Ni_{50}$/Cusil -ABA®/$Ti_{50}Ni_{50}$ specimens infrared brazed at 870 °C for (a) 15, (b) 60, (c) 90, (d) 180 and (e) 300 s.

VAu_2 structure of $TiCu_2$ phase when the x in at.% is higher than ≈ 55, as shown in Fig. 7 [16,17]. Although the binary $TiCu_2$ is a high temperature phase and does not exist at room temperature, it is possible that the $TiCu_2$ phase can be stabilized in a ternary system in which an additional third element is alloyed [16].

3.4. Reaction path of infrared brazed $Ti_{50}Ni_{50}$ alloy

The measurement of dynamic wetting angle demonstrates that the wettability of Ag–Cu eutectic braze on $Ti_{50}Ni_{50}$ substrate can be effectively improved by titanium addition. According to the liquidus projection of Ag–Cu–Ti ternary phase diagram shown in Fig. 8, there is a large miscibility gap in the Ag–Cu–Ti phase diagram [14]. It may play an important role in explaining the mechanism of active brazing.

There are at least three major metallurgical phenomena during infrared brazing, including: melting of the braze alloy, dissolution of the substrate(s) and solidification of the molten braze [7]. All above metallurgical phenomena involve solid–liquid transformation. Additionally, the interfacial reaction between the braze alloy and $Ti_{50}Ni_{50}$ substrate is also involved during the infrared brazing. Therefore, both Ag–Cu–Ti and Cu–Ni–Ti ternary alloy phase diagrams are cited in the study.

The chemical composition of the Cusil-ABA braze in atomic percent is 49.7% Ag, 47.2% Cu and 3.1% Ti as marked by point A in Fig. 8. Since the liquidus temperature of the Cusil-ABA alloy is 815 °C, it can form a homogeneous liquid at brazing temperatures between 840 and 900 °C. The molten braze alloy is readily reacted with $Ti_{50}Ni_{50}$ substrate, and forms interfacial TiCuNi phase as demonstrated in Fig. 4. The presence of interfacial CuNiTi results in isolation of molten

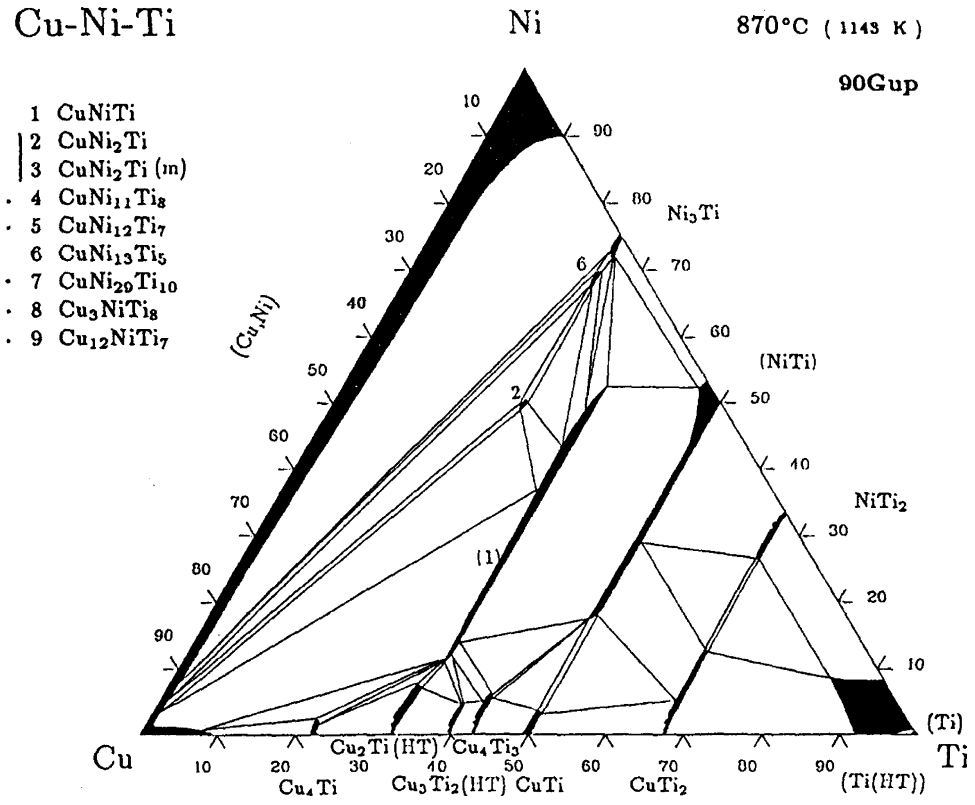

Fig. 5. The isothermal sections of Cu–Ni–Ti at 870 °C in atomic percent [14].

braze during infrared brazing due to its rapid thermal cycle. If the cooling path of the molten braze follows the liquidus projection of Ag–Cu–Ti phase diagram, point A in Fig. 8 moves towards to U_6 and U_7. The reaction scheme of U_6 and U_7 are listed below [14,]:

$$U_6: \quad L + Cu_3Ti_2(HT) \leftrightarrow (Ag) + Cu_4Ti \quad (808\ ^\circ C) \tag{1}$$

$$U_7: \quad L + Cu_4Ti \leftrightarrow (Ag) + (Cu) \quad (783\ ^\circ C) \tag{2}$$

Therefore, the microstructure of the brazed joint is mainly comprised of Ag-rich and Cu-rich phases. This is consistent with the experimental observations.

The chemical composition of the Ticusil braze alloy in atomic percent is 55.3% Ag, 36.5% Cu and 8.2% Ti as marked by point B in Fig. 8. Compared with the Cusil-ABA braze alloy, the amount of Cu is decreased and Ti is increased for the Ticusil alloy. It is also important to note that the chemical composition of Ticusil braze alloy is located inside the huge miscibility gap. Consequently, it is expected that the molten braze tends to be separated into two liquids during brazing. One is rich in Ag, and the other liquid is rich in both Cu and Ti [14,18]. According to Fig. 8, the chemical composition of Ticusil (marked by B) is close to the reaction shown below [14]:

$$L_1'' + CuTi \leftrightarrow L_2'' + Cu_4Ti_3 \quad (900\ ^\circ C) \tag{3}$$

The L_2'' liquid is rich in Ag, and the L_1'' liquid is rich in Cu and Ti. Based on the Cu–Ti binary alloy phase diagram, a series of invariant reactions upon cooling of the Cu–Ti rich liquid are listed below [15]:

$$CuTi + L \leftrightarrow Cu_4Ti_3 \quad (\text{Peritectic},\ 925 \pm 10\ ^\circ C) \tag{4}$$

$$Cu_4Ti_3 + L \leftrightarrow Cu_2Ti \quad (\text{Peritectic},\ 890 \pm 10\ ^\circ C) \tag{5}$$

$$L \leftrightarrow Cu_2Ti + \beta Cu_4Ti \quad (\text{Eutectic},\ 875 \pm 10\ ^\circ C) \tag{6}$$

If the solidification of the Cu–Ti rich liquid follows Eqs. (4)–(6), the formation of interfacial Cu_2Ti phase is caused by peritectic and eutectic reactions as shown in Eqs. (5) and (6), respectively. On the other hand, solidification of the Ag-rich liquid follows Eq. (2), and both Cu-rich and Ag-rich matrix are observed in the experiment (Fig. 6).

Mercier and Melton [10] suggested that the copper solubility in $Ti_{50}Ni_{50}$ is as high as 25 at.% at 155 °C. However, the Ag-rich liquid has little effect on the reaction with TiNi substrate. According to the experimental observation, the Cu–Ti rich liquid preferentially reacts with $Ti_{50}Ni_{50}$ substrate to form interfacial $TiCu_2$ or CuNiTi intermetallics.

For the Cusil-ABA® infrared brazed joint, the Cu-rich phase reacts with $Ti_{50}Ni_{50}$ substrate to form a CuNiTi interfacial layer close to the substrate. This is consistent with Cu–Ni–Ti ternary phase diagram (Fig. 5), because CuNiTi phase shares the phase boundaries with copper and $Ti_{50}Ni_{50}$ simultaneously.

For the Ticusil® infrared brazed joint, the copper content is depleted from the matrix of brazed joint, as illustrated by EMPA analysis results in Fig. 6 due to the formation of interfacial $TiCu_2$ phase, instead of CuNiTi phase. Accordingly, the copper content in the joint is significantly decreased after infrared brazing.

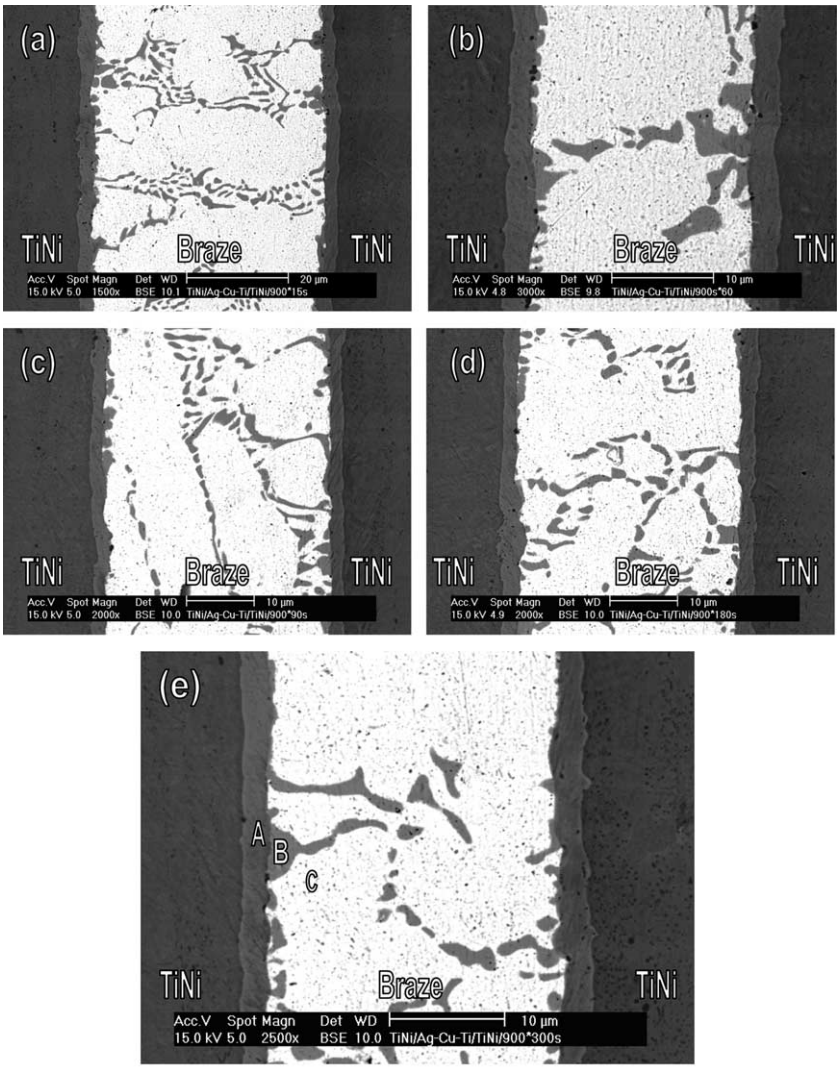

Element (at%)	Cu	Ag	Ti	Ni	Possible phase
A	57.2	1.6	32.9	8.3	$TiCu_2$
B	94.1	4.6	1.3	--	Cu-rich
C	11.1	88.9	--	--	Ag-rich

Fig. 6. SEM BEIs and EPMA chemical analysis results of $Ti_{50}Ni_{50}$/Ticusil®/$Ti_{50}Ni_{50}$ specimens infrared brazed at 900 °C for (a) 15, (b) 60, (c) 90, (d) 180 and (e) 300 s.

3.5. Shape recovery and shear tests of infrared brazed $Ti_{50}Ni_{50}$ alloy

Table 3 summarizes the bending test results for the shape recovery ratio of $Ti_{50}Ni_{50}$ infrared brazed at 840 and 870 °C, for 300 s. The shape recovery ratio of $Ti_{50}Ni_{50}$ base metal is greater than 99%. From Table 3, the shape recovery ratio of infrared brazed joint using Ticusil® filler alloy is much higher than that using Cusil-ABA®. As mentioned earlier, the major difference in the microstructure of infrared brazed joints is the interfacial layer formed near to the $Ti_{50}Ni_{50}$ substrate. The CuNiTi is observed in the case of Cusil-ABA® brazed joint and $TiCu_2$ is in Ticusil®. Yang et al. [8] indicated that the formation of CuNiTi phase in brazing is detrimental to the shape memory effect of $Ti_{50}Ni_{50}$ substrate. Obviously,

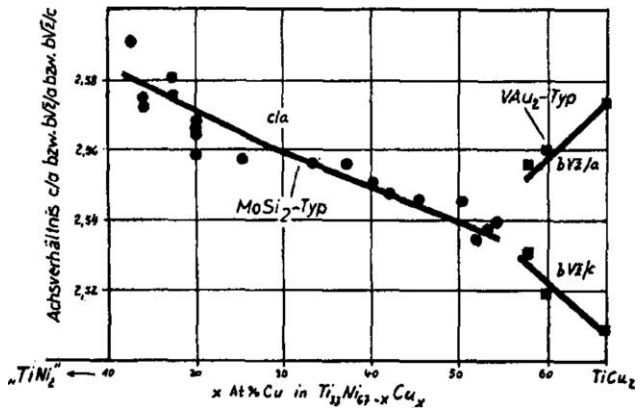

Fig. 7. The $Ti_{33}Ni_{67-x}Cu_x$ structure with variant x at.% of Cu [16].

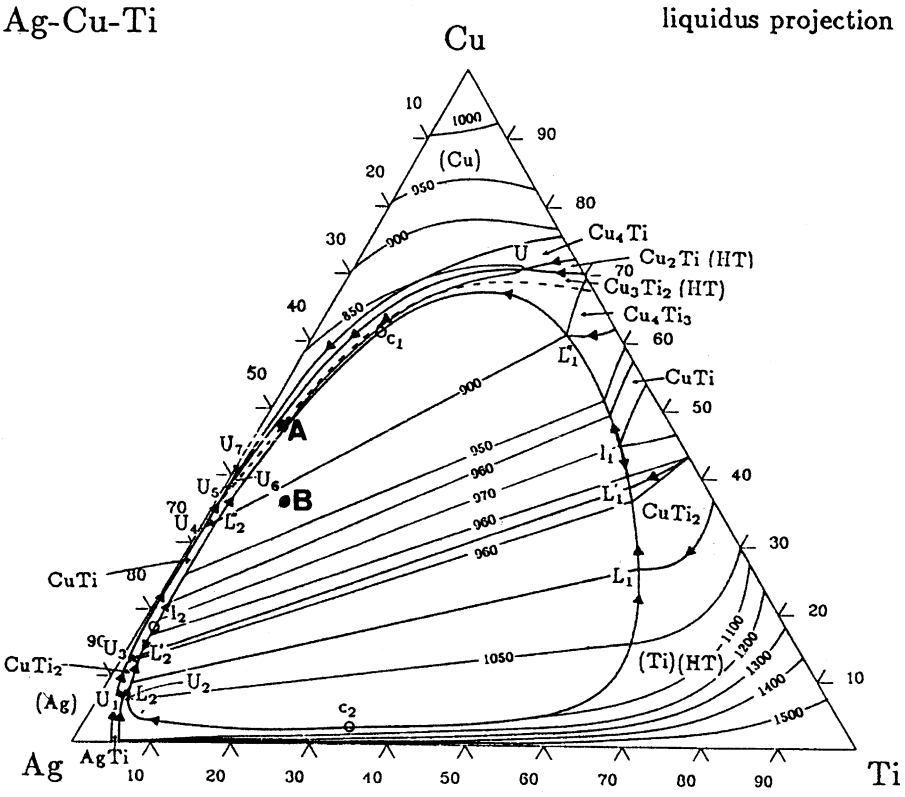

Fig. 8. The liquidus projection of Ag–Cu–Ti ternary phase diagram [14].

the interfacial $TiCu_2$ layer has less damage to the shape memory effect of brazed $Ti_{50}Ni_{50}$ alloy.

The cross-section of the bending test specimen was cut and mounted in an epoxy and then examined by SEM. Fig. 9 shows the SEM images and EPMA results of the specimen infrared brazed at 840 °C and 300 s with Cusil-ABA® braze alloy. The cracks can be observed clearly in the interfacial CuNiTi layer, as indicated by the arrows in Fig. 9(b).

Table 4 shows the shear strengths of specimens brazed at different conditions. The shear strength is 251 MPa for the Cusil-ABA® infrared brazed specimen at 870 °C for 180 s and is 242 MPa for the Tucusil® infrared brazed specimen at 900 °C for 180 s. The brazed joints have their shear strengths higher than 200 MPa if the brazing time exceeds 180 s at 870 and 900 °C, and the variation of shear strength is not obvious due to the absence of significant difference in the microstructures of these infrared brazed joints.

The fractured specimens after shear tests were cross-sectioned and examined by SEM. Cracks can be observed clearly within the brittle interfacial CuNiTi layer for Cusil-

Table 3
Shape recovery ratios of $Ti_{50}Ni_{50}$ base metal and infrared brazed joints using Cusil-ABA® and Ticusil® filler metals

Specimen	Shape recovery ratio $((\theta_i-\theta_f)/\theta_i)$ (%)
50 μm Cusil-ABA® foil at 840 °C for 300 s	64
50 μm Ticusil® foil at 870 °C for 300 s	92
$Ti_{50}Ni_{50}$ base metal	>99

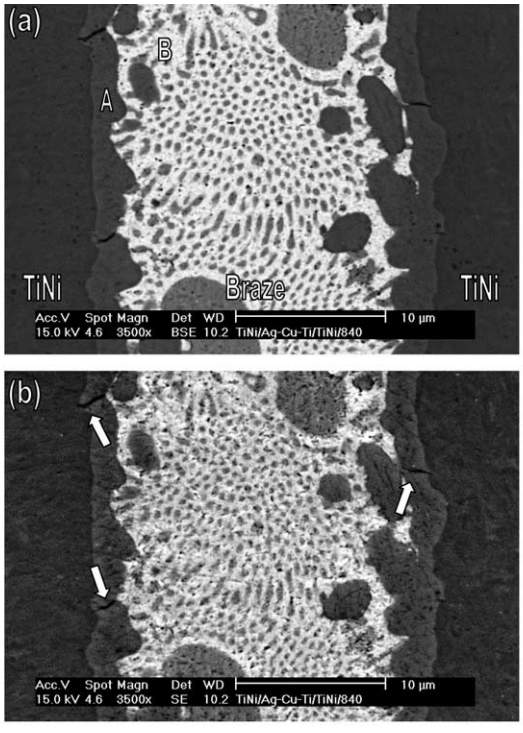

Element (at%)	Cu	Ag	Ti	Ni	Possible phase
A	38.4	--	34.4	27.2	CuNiTi
B	11.4	88.6	--	--	Ag-rich

Fig. 9. Cross-section of bending test specimens and EPMA chemical analysis results of $Ti_{50}Ni_{50}$/Cusil-ABA®/$Ti_{50}Ni_{50}$ infrared brazed at 840 °C for 300 s: (a) BSE and (b) SE image.

Table 4
Shear strengths of joints infrared brazed at various conditions

Brazing time (s)	60	180	300
50 μm Cusil-ABA® foil, 840 °C (MPa)	213	243	173
50 μm Cusil-ABA® foil, 870 °C (MPa)	130	251	225
50 μm Ticusil® foil, 870 °C (MPa)	199	218	214
50 μm Ticusil® foil, 900 °C (MPa)	152	242	208

ABA® brazed joint, as illustrated in Fig. 10. Fig. 11 shows the SEM fractograph and EPMA results of two infrared brazed joints. For the Cusil-ABA brazed joint, the Ag-rich phase shows the dimple dominated appearance, as indicated by Area A in Fig. 11(a). Many cracks in Fig. 11(a) indicated by the arrows are initiated from the brittle CuNiTi phase (Area B) next to the Ag-rich matrix. Similarly, the dimple dominated fracture of the Ag-rich matrix (Area C) and the cleavage fracture of the $TiCu_2$ phase (Area D) are widely observed in Fig. 11(b) for the Ticusil® brazed joint. Accordingly, the presence of interfacial layer in between braze alloy and base metal is detrimental to the bonding strength of the infrared brazed joint.

Fig. 12 shows the XRD results of the fractured surface for $Ti_{50}Ni_{50}$/Ticusil®/$Ti_{50}Ni_{50}$ specimen after shear test. It is clear that strong characteristic peaks of silver and $Ti_{50}Ni_{50}$ substrate are widely observed in the fractured surface. The copper phase is not observed clearly in the fractured surface resulting from the vigorous reaction in braze. The existence of interfacial

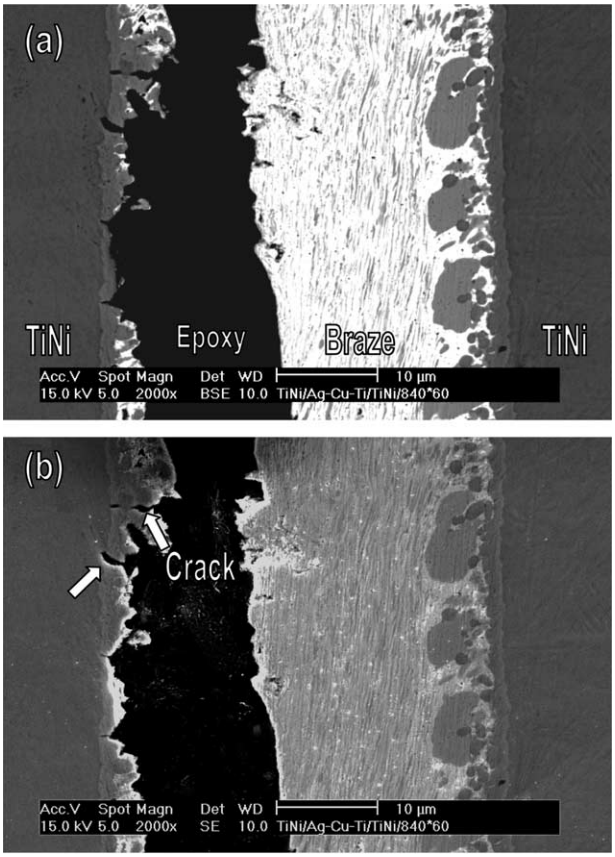

Fig. 10. Cross-section of shear test specimens of ®$Ti_{50}Ni_{50}$/Cusil-ABA®/$Ti_{50}Ni_{50}$ infrared brazed at 840 °C for 60 s: (a) BSE and (b) SE image.

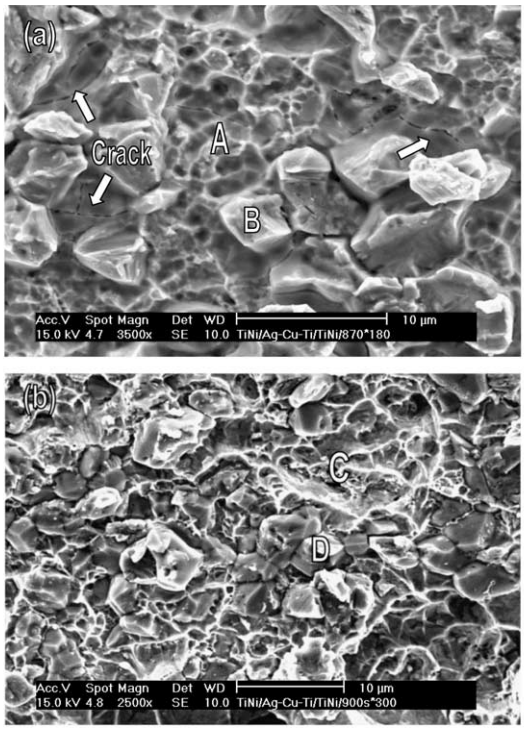

Element (at%)	Cu	Ag	Ti	Ni	Possible phase
A	10.5	89.5	--	--	Ag-rich
B	45.6	--	31.9	22.5	CuNiTi
C	12.8	87.2	--	--	Ag-rich
D	56.1	2.7	32.8	8.4	$TiCu_2$

Fig. 11. The fractograph of shear test specimen and EPMA chemical analysis results of infrared brazed (a) $Ti_{50}Ni_{50}$/Cusil-ABA®/$Ti_{50}Ni_{50}$ at 870 °C for 180 s and (b) $Ti_{50}Ni_{50}$/Ticusil®/$Ti_{50}Ni_{50}$ at 900 °C for 300 s.

$TiCu_2$ phase is confirmed by XRD analysis, as illustrated in Fig. 12, which is in accordance with the aforementioned experimental results.

4. Conclusions

Microstructural evolution, interfacial reaction, shape recovery and shear strength of infrared brazed $Ti_{50}Ni_{50}$ shape memory alloy using Cusil-ABA® and Ticusil® active braze

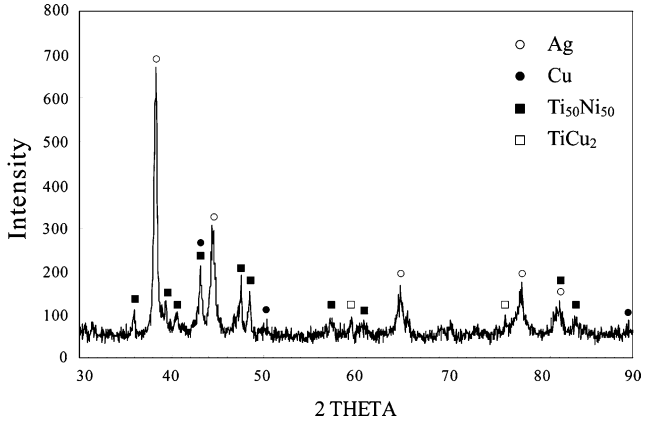

Fig. 12. XRD analysis of the fractured surface after shear test for the $Ti_{50}Ni_{50}$/Ticusil®/$Ti_{50}Ni_{50}$ specimen infrared brazed at 900 °C for 180 s.

alloys are studied. The following conclusions are drawn based on the experimental results.

1. Based on the results of wetting angle measurement, poor wettability of Ag–Cu eutectic braze on $Ti_{50}Ni_{50}$ substrate can be significantly improved by minor addition of titanium into the braze alloy.
2. The infrared brazed $Ti_{50}Ni_{50}$/Cusil-ABA®/$Ti_{50}Ni_{50}$ joint is mainly comprised of Ag-rich, Cu-rich and CuNiTi phases. In contrast, the infrared brazed joint using Ticusil® braze alloy consists of Ag-rich, Cu-rich and $TiCu_2$ phases. Because the chemical composition of Ticusil braze alloy is located inside the huge miscibility gap, the molten braze tends to be separated into two liquids during infrared brazing. One is rich in Ag, and the other is rich in both Cu and Ti. The Ag-rich liquid does not react with $Ti_{50}Ni_{50}$ substrate. In contrast, the copper content is depleted from the matrix of brazed joint due to the formation of interfacial $TiCu_2$ phase.
3. Based on the results of bending test for the shape recovery ratio, the interfacial $TiCu_2$ layer in $Ti_{50}Ni_{50}$/Ticusil®/$Ti_{50}Ni_{50}$ joint is less detrimental to the shape memory behavior than the interfacial CuNiTi layer in $Ti_{50}Ni_{50}$/Cusil-ABA®/$Ti_{50}Ni_{50}$ joint.
4. There is no significant difference in shear strength between these two braze alloys. Both shear strengths are higher than 200 MPa for infrared brazing time exceeding 180 s at 870 and 900 °C. The highest shear strength obtained for Cusil-ABA® braze alloy is 251 MPa at 870 °C for 180 s. Both CuNiTi and $TiCu_2$ interfacial layers are detrimental to the bonding strength of brazed $Ti_{50}Ni_{50}$ joint.

Acknowledgements

The authors gratefully acknowledge the financial support from National Science Council (NSC), Republic of China, under the grant number NSC 93-2216-E-002-008.

References

[1] Miyazaki S, Otsuka K, Suzuki Y. Scripta Metall 1981;15:287–92.
[2] Otsuka K, Shimizu K. Int Met Rev 1986;31:93–114.
[3] Rocher P, El Medawar L, Hornez JC, Traisnel M, Breme J, Hildebrand HF. Scripta Mater 2004;50:255–60.
[4] Filip P, Lausmaa J, Musialek J, Mazanec K. Biomaterials 2001;22:2131–8.
[5] Lin HC, Wu SK. Acta Metall Mater 1994;42:1623–30.
[6] Shiue RK, Wu SK, Chen SY. Acta Mater 2003;51:1991–2004.
[7] Shiue RK, Wu SK, Chan CH. J Alloy Comp 2004;372:148–57.
[8] Yang TY, Shiue RK, Wu SK. Intermetallics 2004;12:1285–92.
[9] Wu SK, Wayman CM. Unpublished work, University of Illinois at Urbana-Champaign; 1984.
[10] Mercier O, Melton KN. Metall Trans 1979;10A:387–9.
[11] Li R, Pan W, Chen J, Lian J. Mater Sci Eng A 2002;A335:21–5.
[12] Paulasto M, van FJJ, Kivilahti JK. J Alloy Comp 1995;220:136–41.
[13] Lin HC, Wu SK. Scripta Metall Mater 1992;26:59–62.
[14] Villars P, Prince A, Okamoto J. Handbook of ternary alloys phase diagrams. Metals Park: ASM International; 1995.
[15] Massalski TB. Binary alloy phase diagrams. Metals Park: ASM International; 1990.
[16] Pfeifer HU, Bhan S, Schubert K. J Less Common Metals 1968;14:291–302.
[17] van FJJ, Bastin GF, Leenen AJH. J Less Common Metals 1978;57:111–21.
[18] Chuang HW, Liaw DW, Du YC, Shiue RK. Mater Sci Eng A 2005;390:350–61.